Durability of Silicate Glasses: An Historical Approach

François Farges[1,2], Marie-Pierre Etcheverry[3,4], Amine Haddi[3], Patrick Trocellier[5], Enzo Curti[6], and Gordon E. Brown Jr.[2,7]

[1] *USM 201 "Minéralogie-Pétrologie", Muséum National d'Histoire Naturelle, CNRS UMR 7160, Paris, France*
[2] *Department of Geological and Environmental Sciences, Stanford University, Stanford, CA, USA*
[3] *Laboratoire des Géomatériaux, Université de Marne la Vallée, France*
[4] *Laboratoire de Recherche des Monuments Historiques, Champs sur Marne, France*
[5] *Service de Recherches de Métallurgie Physique, Commissariat à l' Energie Atomique (CEA), Saclay, France*
[6] *Laboratory of Waste Management, Paul Scherrer Institut (PSI), Villigen, Switzerland*
[7] *Stanford Synchrotron Radiation Laboratory, SLAC, Menlo Park, CA, USA*

Abstract. We present a short review of current theories of glass weathering, including glass dissolution, and hydrolysis of nuclear waste glasses, and leaching of historical glasses from an XAFS perspective. The results of various laboratory leaching experiments at different timescales (30 days to 12 years) are compared with results for historical glasses that were weathered by atmospheric gases and soil waters over 500 to 3000 years. Good agreement is found between laboratory experiments and slowly leached historical glasses, with a strong enrichment of metals at the water/gel interface. Depending on the nature of the transition elements originally dissolved in the melt, increasing elemental distributions are expected to increase with time for a given glass durability context.

Keywords: silicate glasses, melts, weathering leaching, transition elements, XAFS, XANES, microscopies, water, environment.
PACS: 61.43.Fs, 92.60.Sz, 89.60.Gg, 61.10.Ht, 82.20.–w, 68.43.–h, 68.37.–d, 68.37.Yz, 72.15.Cz, 92.40.Lg

INTRODUCTION

Glass resistance to weathering is a concern for geochemists and material scientists (interested in nuclear and municipal wastes) who have conducted a large number of fundamental studies on the dissolution rates of a variety of oxide glasses and the concomitant metal ion leaching that occurs on the glass surface [1-5]. Glass weathering also has a significant impact on historical glasses, particularly stained glasses and archeological glasses. Stained glasses are encountered in monuments (usually religious) from the early Middle Ages to the present, with a large production during the gothic period (XIth-XVth centuries) [5-11]. These stained glasses were mostly exposed to attacks by atmospheric gases. In contrast, archeological glasses are glass-based artifacts found among sepultures, excavations, and other locations where they often occur in soil environments [8]. These artifacts were exposed to chemical corrosion by various fluids and gases for durations lasting from centuries to millenia. This timescale is therefore of special interest because it falls between those achievable in laboratories (days-months-years) [4-5] and those observable in nature (geological glasses weathered over thousands to millions of years) [4]. In addition, historical glasses have unique reaction conditions relative to laboratory-treated and geologic glasses, including exposure to urban environments (dusts, diesel particles, acid rains, mass tourism) and climatic variables (continental vs. temperate, Siberian vs. Mediterranean, etc.) that contribute to their deterioration through chemical and biological processes. Another point of specific importance is the potential lack of accurate knowledge about key parameters controlling the leaching of these historical glasses and all possible human-related processes that might have exacerbated corrosion (e.g., renovations, handling mistakes, variable cultural appreciation concerning value, and intense tourism).

Here we present a brief description of current knowledge of glass durability, with a special focus on historical glasses. We look at the ways synthetic glasses can be weathered in the laboratory and the importance of x-ray absorption spectroscopy to characterize changes. In addition, we present data on various medieval stained glasses that have experienced different climates (Tours basilica (near the Atlantic)

and Strasbourg cathedral (continental)) as well as on archeological glasses from antiquity (Gallo-Roman and Egyptian). A combination of macro- and micro-XAFS/XRF techniques provides a consistent picture of the corrosion history of oxide glasses over this timescale, particularly changes in local coordination environments and spatial distributions of metal cations such as Mn, Fe, and Cu.

Leaching of Silicate Glasses

When exposed to water, the leaching of silicate glasses is thought to involve four different mechanisms. First, the glass surface responds to the stress of a fracture by becoming reactive enough to "sorb" a variety of molecules, mostly atmospheric moieties such as H_2O, CO_2, SO_2, and protons resulting from the hydrolysis of water molecules [10]. Gaseous or dissolved CO_2 and SO_2 moieties form metal carbonates and sulfates on the glass surfaces. Second, dissociated molecules from the fluid phase diffuse inside the fresh glass through a mesoscopic network of fractures. H_3O^+ ions exchange at a very high rate (the "initial rate") with available network modifiers that are water soluble, such as alkalis (but also alkaline-earths and divalent transition elements). This so-called "interdiffusion" effect is initially intense but quickly reaches a steady state with time [5], except possibly in closed systems after long exposures [12]. In a closed system, the pH will locally increase at the interface because of the formation of silanol groups (Si-OH) and the leaching of "free" aqueous ions that were formerly network modifiers [1-7].

The third step is characterized by hydrolysis of the network-formers of the tetrahedral framework of the glass structure, in competition with the previous stage [3]. The formation of these hydrous silica moieties corresponds to a quasi-congruent dissolution of the glass. Until the leached moiety concentrations reach aqueous saturation levels, the glass dissolution rate will decrease as much as the silica concentration in the solution increases. When saturation is reached, the fourth step begins and it involves surface precipitation of hydrolyzed elements that are less soluble. This includes insoluble ions such as Si(IV), Al(III), Fe(III), Ti(IV), REE's, Th(IV), and Zr(IV) that are encountered in many soils resulting from intense tropical weathering (laterites) of primary endogenous rocks. During this stage, a gel phase is formed at the glass/water interface, which is highly hydrous and thus highly sensitive to dehydration. Within soils, the gel will be exposed to concentration and redox gradients and temporal perturbations (among others). Non-steady state conditions will strongly affect these processes, particularly cyclic episodes (such as those produced by seasonal variations), which will induce the formation of layers at the glass surface. More surface precipitates will continue to grow similar to those observed in the first step of glass fracturing; in addition, other crystallites will appear depending on the aqueous chemistry at the glass surface. This evolution suggests that these steps are not well separated in time: they all occur continuously. For instance, the gel/glass interface will penetrate more and more deeply into the mesoscopic fractures of the fresh glass, while precipitates will continue to grow at the water/gel interface. The main parameters that control these processes are (1) glass composition (particularly the aluminum saturation index which is defined as the molar ratio of alumina, Al_2O_3, to the sum of alkali oxides, and the presence of certain elements that enhance (*e.g.,* Na in combination with K, Zr, Zn) or reduce (*e.g*., Mg, Ca in combination with Na) glass durability), (2) tetrahedral polymerization (defined as the non-bridging oxygen per tetrahedron ratio, NBO/T), and (3) physical parameters such as the surface/volume (S/V) ratio, surface microfissurization (Griffith model, related to the melt thermal history, quantified by its glass transition temperature, T_g), and the porosity of the gel layer. Glass weathering will be enhanced with deviations of pH from near neutral values, higher temperatures, and longer exposures to weathering conditions. Until recently, these weathering processes were rationalized in terms of thermodynamic equilibria between the solution and the growing, passivating "gel" on the glass surface [13]. In this model, chemical concentrations at the interface are the primary variables. More dynamic approaches are now considered in modeling these various weathering steps including the physical parameters outlined above (mainly S/V) and also the inherent properties of the "gel". The "gel" is an important additional component of this model in contrast with previous descriptions, which included only the glass and solution phases. The durability of the gel is an important factor in silicate glass weathering because of its sensitivity to changes in water content, its potential to host bacteria and fungi, and its ability to sorb/desorb different moieties. Gels that have formed at the surfaces of various volcanic rocks (mainly ashes and basalts [4]) over geological time scales correspond to maximum weathering rates of 20 µm per 10^3 years [5]. They are rich in silica and Fe(III)-hydroxides.

Laboratory Static Leaching Experiments Probed by XAFS Spectroscopy

Static leaching experiments are used to expose glasses (pellets or powders) to an aqueous solution at a given temperature and pH for a given time period.

Such experiments are typically carried out in a chemically inert container. As shown in Fig. 1, one of the first noticeable changes to the glass surface is fracture filling by various precipitates.

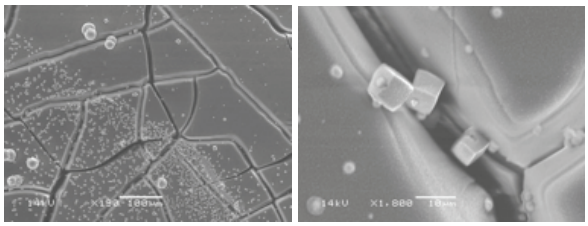

FIGURE 1. Scanning electron microscopy (SEM) images of a weathered glass surface (SON68) (static, 90°C, 28 days, pH=0 and S/V=0.5 cm^{-1}) showing fractures and variably sized crystalline precipitates.

Following this initial surface modification, gels form layers on the glass surface. These gels can be extracted and studied by various microscopies and spectroscopies. These studies have involved mostly highly charged cations, including Fe(III), Zr(IV), Nd(III), and U(VI) [14-16], in dried gels. XAFS studies of these cations at their L_3 edges are difficult and the published interpretations focus on the formation of less soluble and more highly coordinated species. We conducted a series of glass leaching studies under similar conditions but focused on gel dehydration [17-18]. These ion-beam studies (mostly ERDA (energy recoil depth analysis) and RBS (Rutherford backscattering spectroscopy)) have shown the depth of proton diffusion (and resulting hydration) as well as presence of the various transition elements, including Fe, Zr and Mo.

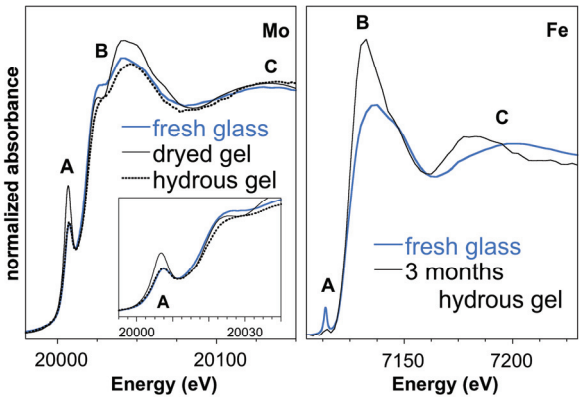

FIGURE 2. (left) Mo K-edge XANES for fresh and aged gel formed on the SON68 glass shown in Fig. 1; the inset is a blow-up of the Mo K-edge pre-edge feature; (right) Fe K-edge XANES spectra for the fresh SON68 glass (prior to exposure to solution) compared with the fresh gel formed on its surface.

Gel Aging

Figure 2 shows the Fe and Mo K-edge XANES spectra collected for the fresh borosilicate glass (SON68), its hydrous gel, and its dried, aged gel (for Mo only).

As seen in Fig. 2 (left), the Mo K-edge XANES of the fresh gel is markedly different from that of the fresh glass. Based on [19], these changes are the result of the formation of 6-coordinated Mo(VI) species in the gel from molybdate ($Mo(VI)O_4^{2-}$) moieties in the fresh glass. In the gel, Mo is most likely present as MoO_3. In addition, the Mo K-XANES of the aged gel is markedly different from that of the fresh gel, particularly in the edge-crest region near 20,040 eV. This difference suggests a more well-defined medium-range environment in the aged gel and more ordered domains around Mo in the dried gel. The Fe K-XANES of the fresh glass indicates mostly tetrahedral Fe(III) in the fresh glass. Following weathering, the pre-edge feature of the hydrous gel is typical of distorted $Fe(III)O_6$ units, as in ferrihydrite (an aperiodic ferric hydroxide or "$Fe(OH)_3$"). With time, ferrihydrite is known to form more ordered varieties of Fe(III)-hydroxides, such as goethite (α-FeOOH).

Long-term Static Experiments

Figure 3 shows a µ-XRF map collected at 1.4 keV using the new LUCIA beamline (now located at the SLS in Switzerland but to be moved to SOLEIL by 2008). The sample studied (MW) is an aggregate of glass grains statically weathered at 90°C for 12 years at the Institut Paul Scherrer in Switzerland [20]. This borosilicate glass contains Mg in contrast to SON68, which is the Mg-free borosilicate glass discussed above.

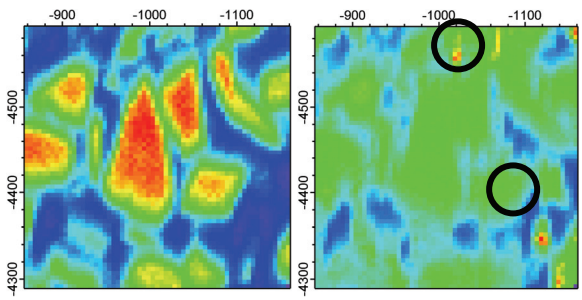

FIGURE 3. µ-XRF maps (300 x 300 µm; 5x 5µm spot; LUCIA, SOLEIL-SLS) for the Na-K_α radiation (left) and Mg-K_α (right) for a borosilicate glass (MW) weathered statically for 12 years at PSI (Switzerland). Relative color maps range from dark (blue) (low concentration) to bright (red) (high concentration).

The maps in Figure 3 show the distribution of Na (left) and Mg (right) in weathered MW glass. The

glass section is 40 µm thick, and the average grain size is about the same thickness. Because of the softness of the x-rays, these XRF maps probe only a few microns into the glass sample. Note the zoning of Na in each grain, which highlights the preferential leaching of Na as compared to Mg, which shows little zoning. In addition, Mg shows some hot spots that are newly formed precipitates. Their Mg K-edge µ-XANES (Fig. 4) is similar to that of talc ($Mg_3Si_4O_{10}(OH)_2$). This XANES is also similar to Mg-rich crystallites of montmorillonite, a related phyllosilicate of composition ~$(Na,Ca)_{0.3}(Al,Mg)_2Si_4O_{10}(OH)_2 \cdot n(H_2O)$ that was found by TEM in this sample [21]. Comparison of Mo and Fe in SON68 (after 3 months of leaching) vs. Mg in MW (after 12 years of leaching) shows that metal-rich crystallites are formed on both glass surfaces. These results indicate that the weathering mechanisms for borosilicate glasses subjected to leaching experiments ranging from 3 months to 12 years are similar. Drying has a major effect on the local structural environments of transition elements in the gels formed on these glasses, so special care is required to study gels under environmental conditions.

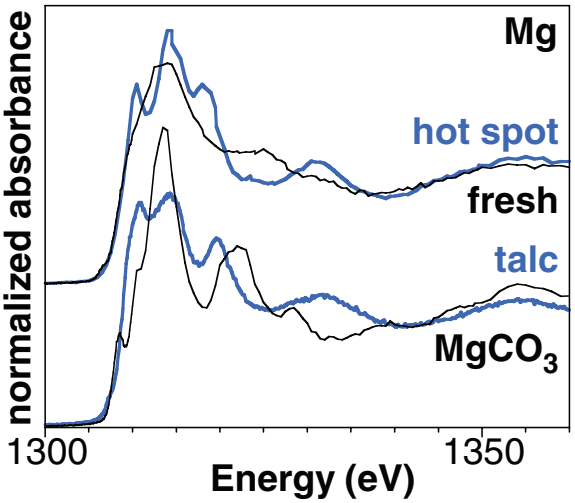

FIGURE 4. Mg K-edge µ-XANES spectrum (LUCIA beamline) of the non-leached MW glass compared with that of the Mg-rich spot shown in Fig. 3 (right) and with the Mg K-XANES of $MgCO_3$ (magnesite) and talc.

Historical Glasses

In brief, two types of historical glasses are known which have experienced long-term weathering: stained glasses and archeological glasses. Stained glasses are (or were) exposed for significant durations to both rainwater (on the outside of the building) and moisture (on the inside of the building). These glasses are also exposed to atmospheric particulates such as dusts from urban environments (diesel particles, dusts enriched in sulphates from combustion of wood, coal, candles) [10] as well as sea salts when they are located close to seashores [22]. Weathered archeological glasses are usually found buried in sepultures and were exposed to chemical and microbiological interactions in soils [8].

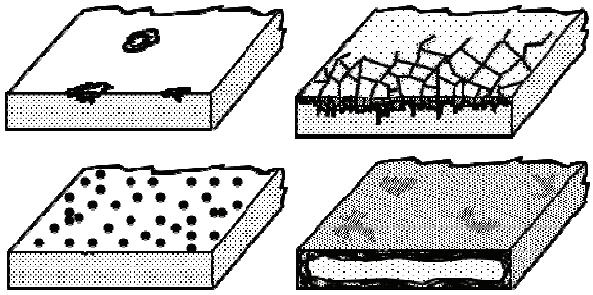

FIGURE 5. Schematic representation for the four main types of historical glass corrosion and their principal causes: (left, top) corrosion cupules (condensation, inside buildings); (left, bottom) surface aggregates from atmospheric dusts (inside/outside); (right, top) fractures and in-depth corrosion (exposure to rain water); (right, bottom) archeological corrosion by pore water (+ bio-organic agents) as in a soil. Modified after [8] (with permission).

The Saint Gatien Basilica in Tours

This basilica is located in the Loire Valley of France and is exposed to the moderating climatic influences of the Gulf Stream because of its relative proximity to the Atlantic Ocean. The stained glass windows of this basilica show corrosion cupules on the inside and highly weathered layers on the outside (Fig. 6).

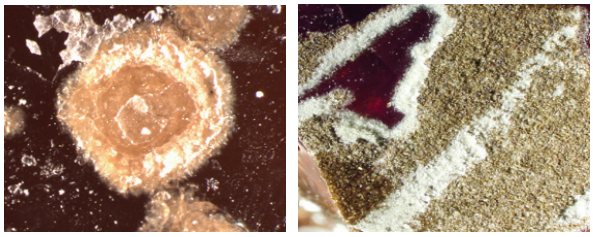

FIGURE 6. Optical images of two sides of a red-stained glass from the Tours basilica: (left) corrosion cupules (1 mm in diameter); (right) weathered layer (~500 µm thick), covering the original red glass (appearing in the left top corner because of an indent; 5 mm long).

The red-stained glasses of the Tours basilica are from the XIVth century. Their red color is due to copper nanoparticles [23]. In cross section, these glasses consist of a 500 µm-thick layer composed of micron- thick layers of deep red and pale-green glasses (named "*feuilleté*"). This *feuilleté* is deposited on a

few mm-thick pale green glassy substrate. The thin red *feuilleté* layer is sufficiently intense in color to give the entire thickness of glass a red color in transmission. This red layer is weathered and forms a dominantly brownish crust with pale-blue stripes (Fig. 6, right). Figure 7 shows the XRF image of the structure of this composite sample, with the red feuilleté layer surrounded by the greenish substrate (top) and the brownish crust (bottom). µ-XRF maps were collected at the 10.3.2 beamline of the ALS.

The feuilleté region of the cross section is enriched in Cu (in contrast to the greenish layers). Cu K-edge µ-XANES spectra confirm that Cu is dominantly monovalent is these glasses (see [23] for details) with ~10 atom% of the Cu occurring as metallic aggregates and causing the red color of these glasses. In contrast, Cu is divalent in the weathered brownish crust (spot #5 in Fig. 7).

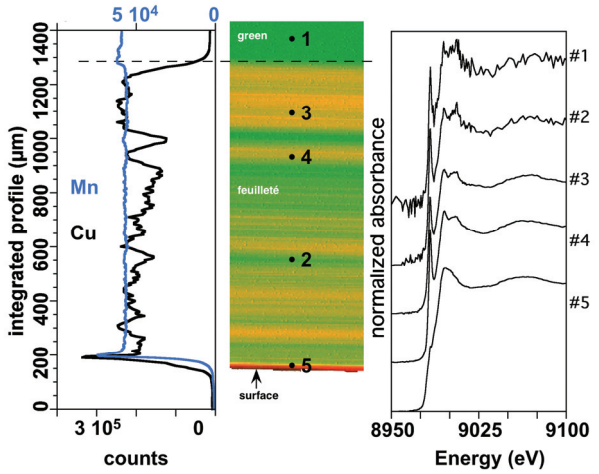

FIGURE 7. X-ray fluorescence image (10 keV) of a cross section of a red-stained glass from the Tours basilica (center); the integrated Cu Kα and Mn Kα profiles (left); and five Cu K-edge µ-XANES spectra in selected areas of the cross section: the greenish substrate (top, x1), a deep red layer inside the *feuilleté* layer (middle, x3) and the brownish crust (bottom, x1).

As shown in Fig. 7, the Cu K-edge µ-XANES for spot #5 (as well as its µ-EXAFS spectrum [23]) is similar to that of chalcanthite ($CuSO_4$•$5H_2O$). Indeed, sulfate-rich crusts on the stained glasses are typical at the Tours basilica [22] and can be related to the relative proximity to the Atlantic Ocean and the climatic influence of the Gulf Stream. Na and Mn K-edge µ-XANES spectra (Fig. 8) on the sulfate-rich crust of the same stained glass, show significant enrichment in Na and Mn (in addition to Cu; see Fig. 7). The Mn K-edge XANES for the crust is shifted to higher energies as compared to the non-leached glass. The Mn K-edge µ-XANES spectrum for the fresh glass is typical of divalent Mn [24]. The Mn K-edge XANES for the crust is similar to that measured for phyllomanganates such as birnessite [24-25], suggesting an average Mn valence between 3.5 and 4. The Na K-edge XANES spectra for the non-leached glass and its surrounding crust are similar in shape and a reliable interpretation requires further *ab-initio* XANES simulations.

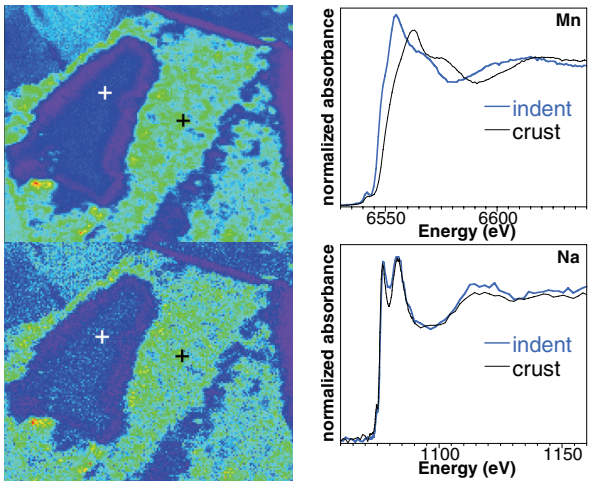

FIGURE 8. Na K_α and Mn $L_{\alpha/\beta}$ (at 1.4 keV) XRF maps (left), and Na and Mn µ-XANES (right) of the surface of one stained glass from the Tours basilica (black/blue=low; white/green=high). The spectra were collected in the indent area (see crosses on the top left image) of the fresh glass and in the brownish crust around that indent. Similar positions were probed at the Mn K-edge.

The Notre Dame Cathedral in Strasbourg

The stained glasses of the Notre Dame cathedral in Strasbourg show a type of deterioration different from that observed in the Tours basilica: intense darkening due the formation of black crusts. This deterioration is a major contributor to the reduced light transmission through the stained glass to the interior of the building. As for the Tours basilica, a combination of various methodologies was employed to understand the origin of the stained glass darkening. Optical and electronic observations of the same sample from the Notre Dame cathedral in Strasbourg show that a 1 mm-thick crust is present on the stained glass surface. This crust shows horizontal layers of varying brown colors. No clear evidence for a deep black crust was observed at this scale, in contrast to unmagnified observation by eye. Figure 9 shows the SEM and µ-XRF images collected for a black crust from a cross-section of a stained glass from the Notre Dame cathedral of Strasbourg.

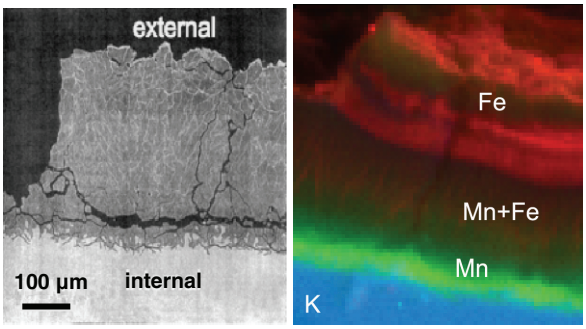

FIGURE 9. SEM (left) and µ-XRF (right, 400x400 µm; pixel=5x5 µm) images collected for the black crust from a stained glass from the Notre Dame cathedral of Strasbourg. The (artificial) colors of the µ-XRF map (LUCIA beamline) are medium gray/blue for K, white/green for Mn and dark gray/red for Fe.

The µ-XRF image was collected at the LUCIA beamline with 7.2 keV x-rays. This XRF image shows layers parallel to the glass surface. The thicker layer (a dried gel) is enriched in iron, whereas a deeper layer is enriched in manganese. The deepest portion of the non-leached glass from the XIVth century is rich in K. Note that these interfaces do not appear in SEM images, which are more sensitive to percolation features oriented normal to the glass surface (the larger dark cracks are related to sample preparation artifacts).

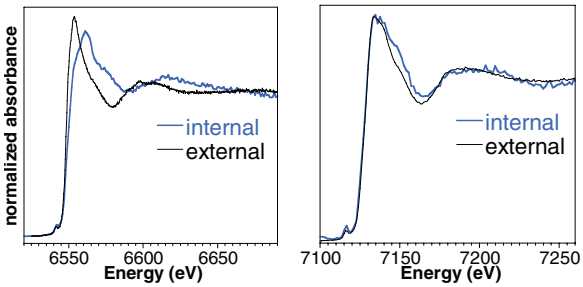

FIGURE 10. Mn (left) and Fe (right) K-edge µ-XANES spectra for the same stained glass cross section from the Notre Dame cathedral as shown in Fig. 9. The spectra were collected for two spots located in the Fe-rich crust (external; see Fig. 9 (left)) and in the Mn-rich (internal) layers.

Mn and Fe K-edge µ-XANES spectra were collected from each side (external and internal) of the crust (Fig. 10). Mn is oxidized (from 2+ to 3.5+) during weathering of the ancient glass and forms phyllomanganate-type compounds. Iron is also oxidized (from 2+ to 3+) and forms ferrihydrite-type compounds, which are very dilute in the "internal" side of the crust (Mn-rich). These results indicate that two different layers comprise the crust: a thick one rich in Fe(III)- and Mn(II, III, IV)-oxyhydroxides, and a thin one (enriched in Mn(II, III, IV)). Given the respective colors of Fe- and Mn-oxyhydroxides, it is clear that the manganese-rich ones are the dominant cause of the black color of this ensemble. A major finding is that the darkest layer is the deepest and remained undetected by previous, more conventional analyses. Further work is in progress to understand the origin of that buried Mn-rich layer and possible microbiological processes that may have caused it.

Archaeological Glasses

The Egyptian blue pigment from St. Romain-en-Gal is a high-temperature mixture containing both crystalline cuprorivaite ($CaCuSi_4O_{10}$) and a Cu(II)-bearing glass [27]. This pigment was prepared during the Gallo-Roman period (100 BC) in the southern area of Lyon (France). This site is close to the Rhône river and was constantly saturated with pore waters for 2000 years. Here, cuprorivaite crystals, surrounding pockets of interstitial glass, comprise the pigment. SEM images (Fig. 11) show that the confined glass is extensively weathered with compositional zoning [27].

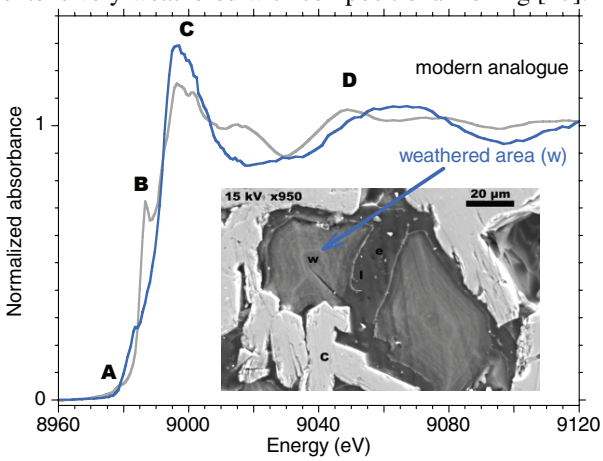

Figure 11. SEM image of a weathered interstitial glass from an Egyptian blue pigment from the Gallo-Roman site of St. Romain-en-Gal site (2000 years old). The Cu K-edge XANES spectrum (black) for the weathered area is typical of Cu(II) (the Cu K-edge XANES spectrum for a modern analog of that former glass - in grey – indicate more Cu(I)).

Compositional profiles show that Si is enriched at the center of the regions shown in Fig. 11, whereas Cu is highly concentrated at their rims (more than 40 wt.% Cu). The analogy with stained glasses is remarkable: pore waters affect archeological glasses like rainwater for stained glasses and geological glasses. A Si-rich region (formerly a gel) is present and metals are highly enriched at its periphery. Because of the longer and more corrosive exposure of archaeological glasses in soils, relative to stained cathedral glasses, the Si-Cu distribution is more pronounced, compared to the stained glasses of the Tours basilica.

A glass from a Sekhmet statue (XIXth dynasty, sampled during the XIX century [27]) was also

examined. This sample is a Cu-bearing glass that was confined for 3000 years in the dry climate of the Libyan desert (West of the Nile river). Figure 12 shows µ-XRF/µ-XANES data for this sample and a modern replica of this glass, based on electron microprobe analyses of this sample. The ancient material appears to be compositionally homogeneous, and its copper speciation indicates that Cu(I) was oxidized in Cu(II) over time, without other significant changes in the glass structure and composition (*e.g.*, not hydrated) [27]. The location of these Ca-rich glasses in such a dry climate resulted in a low degree of weathering over 3000 years. In contrast, the St. Romain-en-Gal sample (Fig. 11) is highly weathered.

XAFS spectroscopy can be used to distinguish between such ancient and modern artifacts, based simply on the Cu(II)/Cu(I) ratio. Silicate glasses high in Cu(II) are difficult to prepare except by complex implantation/diffusion experiments and thus can not be easily synthesized by those who replicate ancient artifacts [28]. As an additional benefit, the approach used here provides a new way to identify fake Egyptian artifacts based on Cu K-edge pre-edge XANES features.

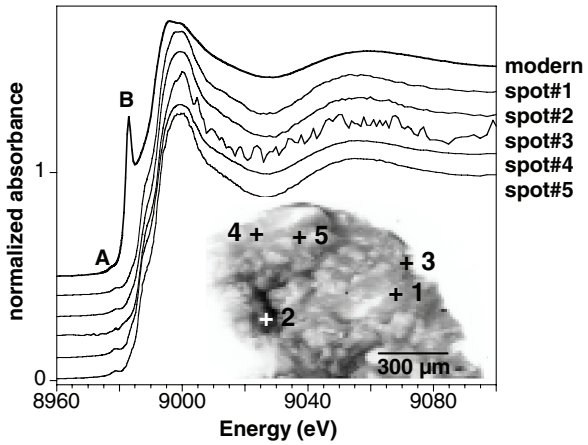

Figure 12. µ-XANES spectra (Cu K-edge) for a bluish enamel covering a Sekhmet statue of the XIXth dynasty (µ-XRF map at 10 keV shown in the inset). Also shown is a XANES spectrum of a modern replica of the glass phase.

CONCLUSIONS

Analyses of modern and ancient glasses provide detailed information that helps us understand weathering processes over centuries and millenia [1-10]. XAFS spectroscopy in particular shows that metals (Mn, Fe, Cu) form hydroxide phases at the gel/solution interface, and this phenomenon is enhanced with gel ageing. Depending on the nature of the transition elements originally dissolved in the melts, local metal enrichments are expected to increase in these materials with time due to dissolution/ precipitation processes. Micron-scale studies of the weathering of historical glasses can provide important information on glass durability over time periods ranging from thousands to hundreds of years, and thus can be useful in better understanding the factors controlling the durabilities of glasses used to encapsulate nuclear and municipal wastes.

ACKNOWLEDGMENTS

This research was supported in part by NSF Grant CHE-0431425 (Stanford Environmental Molecular Science Institute).

REFERENCES

1. C.J. Hench and D.E. Clark, *J. Non-Crystall. Sol.* **28**, 83 (1978).
2. R.H. Doremus, *J. Non-Crystall. Sol.* **19**, 137-144 (1975).
3. R. Boksay *et al.*, *Phys. Chem. Glasses* **9**, 69-71 (1968).
4. J.L. Crovisier, T. Advocat and J.L. Dussossoy, *In* "Energy Waste and the Environnement - A Geochemical Perspective". Geological Society Special Publication **236** (R. Giéré & P. Stille Eds), 113-121 (2004).
5. E. Vernaz *et al.*, *J. Nucl. Mater.* **298**, 27-36 (2001).
6. U. Braeutigam *et al.*, *Glass Sci. Technol.* **68**, 29-33 (1995).
7. R. Newton and S. Davidson, Conservation and Restauration of Glass, Butterworth-Heineman, Oxford, 318 pp. (2003).
8. J. Sterpenich and G. Libourel, *Chem. Geol.* **174**, 181-193 (2001).
9. H. Römich, Historic glass and its interaction with the environment. In N.H. Tenet, Ed., "The Conservation of Glass and Ceramics", pp 5-14. James and James (Science Publishers), London (1999).
10. M. Melcher and M. Schreiner, *Anal. Bioanal. Chem.* **379**, 628-639 (2004).
11. I. Pallot-Frossard and M.-P. Etcheverry, *Rev. Staz. Sper. Vetro* **35**, 1118-1129 (2005).
12. B. Grambow and R. Muller, *J. Nucl. Mater.* **298**, 112-124 (2001).
13. P. Aagard *et al.*, *Amer. J. Sci.* **282**, 237-285 (1982).
14. E. Pelegrin, PhD thesis, Univ. Paris 7 (2000).
15. P. Jollivet, *J. Nucl. Mater.* **301**, 145-152 (2002).
16. P. Jollivet, *J. Nucl. Mater.* **346**, 253-265 (2005).
17. A. Haddi *et al.*, *Nucl. Instr. & Meth. B* **249**, 869-873 (2006).
18. P. Trocellier *et al.*, *Nucl. Instr. & Meth. B* **240**, 337-344 (2005).
19. F. Farges, *Can. Mineral.* **44**, 731-754 (2006).
20. E. Curti, Techn. Bericht – Nagra NTB, 21 (2003).
21. E. Curti *et al.*, *Appl. Geochem.* **21**, 1152-1168 (2006).
22. R.A. Lefevre *et al.*, *Glass Sci. Technol.* **71**, 75-80 (1998).
23. F. Farges *et al.*, *Appl. Geochem.* (in press).
24. F. Farges, *Phys. Rev. B* **71**, 155109 (2005).
25. A. Manceau *et al.*, *Geochim. Cosmochim. Acta*, **66**, 2639-2663 (2002).
26. M.P. Etcheverry, PhD thesis, Univ. Bordeaux (1999).
27. C. Maurizio *et al.*, *Europ. Phys. J. B* **14**, 211-216 (2000).